ACS OMEGA

Open Access

http://pubs.acs.org/journal/acsodf

Review

Comprehensive Review on Downconversion/Downshifting Silicate-Based Phosphors for Solar Cell Applications

Abinaya Mayavan*

Cite This: *ACS Omega* 2024, 9, 16880−16892

Read Online

ACCESS | Metrics & More | Article Recommendations

ABSTRACT: Insufficient utilization of the solar spectrum in commonly employed solar cells, stemming from a spectral mismatch between the solar spectrum and the solar cell's band gap, poses a barrier to enhancing solar cell efficiency. To overcome this challenge, downconverting silicate phosphors are employed in solar cells to capture the infrared spectrum of sunlight, thereby augmenting solar cell efficiency. Downconversion/downshifting involves in converting high-energy photons into one or two near-infrared (NIR) photons. Remarkably, silicate-based downconverting phosphors enhance solar cell sensitization, light scattering, antireflectivity, and stability. This review delves into the various energy transfer mechanisms utilized in silicate phosphors. The key aspects covered in this review encompass the development of silicate phosphors that emit NIR light and their synthesis process. The working principle of the solar cell and its parameters are discussed. The impacts of silicate phosphor size, coverage, volume concentration, and arrangement on solar cell performance are also explored. Furthermore, the study addresses several intriguing approaches for developing innovative silicate phosphors to enhance solar cell performance.

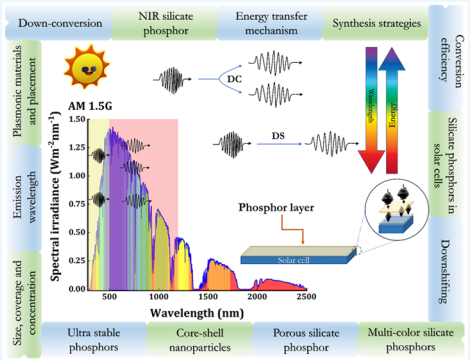

1. INTRODUCTION

Renewable solar energy is gaining significant attention among researchers. This is due to the need to move away from a carbon-based energy economy, consistent with ongoing efforts to achieve global sustainability.[1] Solar energy offers a promising way forward, and India is significantly interested in this direction.[2] Research is ongoing on next-generation solar cells that are fabricated using dye-sensitized colloidal TiO_2,[3−6] silicon,[7−10] perovskite,[11−14] and organic-based materials.[15−18] From an industrial standpoint, however, silicon photovoltaics (PVs) continue to be the preferred option. In fact, they alone occupy about 90% of the PV market[19] owing to silicon's merits; viz., it is nontoxic, an ample element in the earth, an elemental semiconductor, and so on.

Solar cells, in general, have their best spectral response at longer wavelengths (950−1100 nm). The high-efficiency architectures find a limited consumer base, though, owing to their prohibitive costs. Hence, PVs continue to dominate the market. However, these are deficient in terms of their efficiencies. They encounter energy losses: (1) Optical losses include reflection from a module's surface interface. (2) The use of poor-quality materials results in recombination loss. (3) Sub-band-gap energy photon loss occurs when photon energy is insufficient to activate the semiconductor and produce pairs of electrons and holes. (4) High energy can only transfer one electron to the conduction band, and excess energy is lost as heat (thermalization).[20−22] Under nonconcentrated AM1.5 light, these fundamental losses directly result in an efficiency limit of 30% for all commonly used single-junction solar cells.[23]

Improving PV efficiency is an urgent need. To reduce thermalization losses, phosphors have been employed with solar cells, to achieve relevant wavelength conversion, thereby allowing for improvement in efficiencies.

An extensive class of phosphors or luminescent materials is a matrix, consisting of activators and a transparent host. Typically, other types of impurities are codoped when the activators have a weak absorption cross section. These impurities absorb the excitation energy and then transfer it to the activators. These second-doped ions are usually referred to as sensitizers.[24−26]

Transition metal and lanthanide ions are the two types of metal ions that are commonly used as impurities. Transition metal ions involve d−d transitions. In lanthanide ions, parity allowed 5d−4f and parity forbidden 4f−4f occur and are responsible for luminescence emission.[27] The broad range of applications of metal-ion-doped luminescent materials, spanning from optoelectronics to biomedicine and nearly every facet of human existence, has garnered significant interest.

Received: November 5, 2023
Revised: March 20, 2024
Accepted: March 22, 2024
Published: April 6, 2024

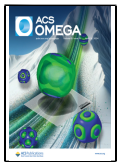

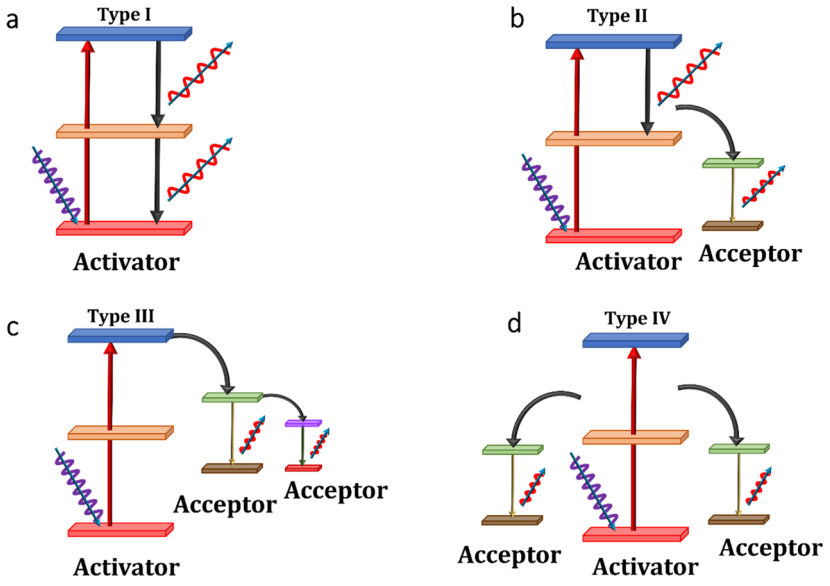

Figure 1. Energy level diagrams of various downconversion processes in silicate phosphor.

Phosphor is involved in three kinds of luminescence processes: (1) downconversion; (2) upconversion; (3) downshifting. The downconversion process involves the conversion of high-energy photons to low-energy photons (i.e., UV to visible/near-infrared red light).[28] Under Stokes' law, the downshifting process involves a change in wavelength and is analogous to the downconversion process (i.e., higher energy is converted to lower energy).[29] The process involved in upconversion converts low-energy photons to high-energy photons (i.e., infrared or near-infrared light to visible/UV light).[30]

The solar cell with a combination of downconverting material showed an efficiency greater than 100%. Energy loss from high-energy photon absorption is prevented in solar cells when downconverted photons are absorbed rather than high-energy photons. Considerable enhancements in efficiency are observed for solar cells with a band gap energy of 1.1 eV. The downconverting layer on the back surface of a solar cell is found to have an upper limit of 39.63%, reported by Trupke et al.[31] There have been several reports on the use of downconversion phosphors (aluminate, silicate, garnet, and so on) in solar applications. Because of their thermal and chemical stabilities, silicates are regarded as the most reliable host materials for persistent luminescence.[32,33] Moreover, they offer high quantum efficiency, a large band gap, and color-tunable properties.

Based on this survey, the present work highlights the advances in silicate downconversion materials to improve the performance of different solar cells. This review article is organized as follows: In section 2, an overview of the mechanism behind the downconversion material is provided. The methods developed to synthesize the downconversion material are described in section 3. In section 4, the different kinds of silicate materials so far developed are discussed. In section 5, the basic working principle of solar cells and their parameters are discussed. In section 6, the application of silicate materials to solar cells' conversion efficiency is analyzed via phosphor size, coverage, emission wavelength, arrangement, and so on. Finally, this work ends with a summary and prospects of the review article.

2. ENERGY TRANSFER MECHANISM OF NIR SILICATE PHOSPHOR

The downconversion/downshifting phosphors works via large Stokes' emission, in which activator ions absorb UV photons and emit visible to near-infrared photons. Dexter discovered this phenomenon, which is also known as quantum cutting, in 1953.[34] It is accomplished by the cascade emission of photons from a single lanthanide ion or through downconversion via energy transfer with distinct sets of lanthanide ions.

The type of energy transfer mechanism between the activator and sensitizer is summarized and shown in Figure 1. Type I involves ground state absorption as shown in Figure 1a. The single activator ion is responsible for emitting two NIR photons after absorbing UV photons. The single emitting ion returns to its ground state due to a shorter population of the intermediate level leading to undesirable emissions in the spectral range of UV−vis.

The use of two activator ions in downconverting materials is involved in the alternative energy transfer mechanisms as illustrated in Figures 1b,c. The activator transfers its energy to one of the acceptor centers. Then the acceptor center can deexcite by cross-relaxation, causing another adjacent acceptor ion to become excited. Two NIR photons are produced because of this mechanism. It is ideal for NIR quantum cutting. This process involves resonance energy transfer (RET) and takes place via one (type II) and two (type III) step energy transfer. Figure 1b,c display the emission of two NIR photons via one- and two-step energy transfer.

Figure 1d displays type IV as a cooperative energy transfer mechanism (CET). The excited state energy of the activator is divided into two photons and transferred to two neighboring acceptor centers, resulting in two emitting NIR photons.

To further investigate the type of energy transfer mechanism, the critical distance (R_c) between the activator ions is calculated. The oxide phosphor usually undergoes nonradiational energy transfer via exchange interaction or multipole−multipole interaction. If the distance between the activator is greater than 5 Å, energy transfer might occur due to multiple−multipole interaction. R_c can be calculated via the concentration quenching method by the Blass equation,[35−37] as follows:

https://doi.org/10.1021/acsomega.3c08806
ACS Omega 2024, 9, 16880−16892

Table 1. NIR Emitting Silicate Phosphor and Its Parameters

PSR	SS	T (°C)	t (h)	λ_{ex} (nm)	λ_{em} (nm)	ET	SM	IQE (100%)	ET (100%)	$I_{150\,°C}$ (100%)	ref
Li_2SrSiO_4:0.06Ce^{3+},0.06Pr^{3+}	SSR	880	4	360	450−1100	CET	NNI	–	20.00	–	60
Sr_2SiO_4:0.04Ce^{3+},0.06Tb^{3+},0.03Yb^{3+}	SSR	1100	3	350	400−1100	RET	DDI	–	50.00	–	61
Ba_2SiO_4:0.03Eu^{2+},0.03Nd^{3+}	SSR	1250	6	400	500−1100	RET, CET	–	–	78.90	–	62
Mg_2SiO_4:0.1Cr^{3+},Cr^{4+}	SSR	1250	5	470	650−1400	–	–	–	–	–	63
$NaAlSiO_4$:0.1Er^{3+},0.005Yb^{3+}	SSR	1300	5	380	700−1600	RET	–	–	–	–	64
Sr_3SiO_5:0.025Ce^{3+},0.05Al^{3+},0.025Nd^{3+}	SSR	1450	4	410	450−1100	RET	–	–	66.52	–	65
$Y_2CaAl_4SiO_{12}$:0.06Cr^{3+}	SSR	1550	4	440	600−1100	–	–	75.90	–	85.00	66
$Y_2SrAl_4SiO_{12}$:0.05Ce^{3+},0.03Cr^{3+}	SSR	1500	4	460	500−800	–	QQI	72.88	49.69	38.00	67
$Y_3MgAl_3SiO_{12}$:0.03Ce^{3+},0.01Cr^{3+}	SSR	1570	4	435	650−950	–	DDI	–	–	75.00	68
$Y_3Ga_3MgSiO_{12}$:0.04Cr^{3+}	SSR	1400	5	438	650−1100	–	–	79.90	–	84.40	69
$Na_2CaGe_5SiO_{14}$:0.08Cr^{3+}	SSR	1050	8	419	600−900	–	–	–	–	–	70
$LiInSi_2O_6$:0.06Cr^{3+}	SSR	1050	10	460	700−1100	–	–	–	–	77.00	71
$NaScSi_2O_6$:0.04Cr^{3+}	SSR	1200	5	460	700−1100	–	NNI	–	–	–	72
$LiScSi_2O_6$:0.1Cr^{3+}	SSR	1200	5	460	700−1100	–	NNI	–	–	–	72
$NaScSi_2O_6$:0.04Cr^{3+},0.005Li	SSR	1200	5	460	700−1100	–	–	22.20	–	69.00	72
$LiScSi_2O_6$:0.1Cr^{3+},0.02Li	SSR	1200	5	460	700−1100	–	–	64.40	–	75.00	72
$LiScSi_2O_6$:0.06Cr^{3+},0.14Yb^{3+}	SSR	1200	10	468	700−1100	–	–	65.40	94.50	62.00	73
$K_3ScSi_2O_7$:0.03Eu^{2+}	SSR	1050	6	465	600−1000	–	–	–	–	70.40	74
$Ca_4Si_2O_7F_2$:0.06Ce^{3+},0.4Er^{3+}	SSR	1000	15	380	400−1600	–	DDI	–	71.00	–	75
$CaAl_2Si_2O_8$:0.07Ce,0.1Tb,0.06Yb	SSR	1350	50	315	380−1100	RET, CET	–	–	–	–	76
$Ca_2LuScAl_2Si_2O_{12}$:0.02Cr^{3+}	SSR	1400	6	442	600−900	–	NNI	73.70	–	76.00	77
$BaZrSi_3O_9$:0.07Cr^{3+}	SSR	1500	5	455	700−1000	–	DDI	–	–	–	78
$BaZrSi_3O_9$:0.005Cr^{3+}	SSR	1350	4	458	650−1200	–	–	7.00	–	59.00	79
$BaSnSi_3O_9$:0.01Cr^{3+}	SSR	1300	4	449	650−1200	–	–	16.00	–	38.00	79
$BaHfSi_3O_9$:0.03Cr^{3+}	SSR	1300	4	460	650−1200	–	–	13.00	–	43.00	79
$(Y,Ba)_3(Al,Si)_5O_{12}$:0.03Ce^{3+},0.1Cr^{3+}	SSR	1480	4	467	500−800	–	DDI	63.40	–	77.00	80
$Lu_2CaMg_2Si_3O_{12}$:0.05Cr^{3+}	SSR	1350	5	450	650−1000	–	DQI	76.00	–	70.00	81
$Ca_3Sc_2Si_3O_{12}$:0.06Ce^{3+},0.03Cr^{3+}	SSR	1400	6	460	470−900	–	DDI	83.80	41.00	82.00	82
$Ca_3Sc_2Si_3O_{12}$:0.06Ce^{3+},0.03Cr^{3+},0.05Nd^{3+},0.03Yb^{3+}	SSR	1425	8	450	480−1100	RET	DDI	–	–	79.00	83
$Ca_3Sc_2Si_3O_{12}$:0.03Cr^{3+}	SSR	1500	3	460	700−900	–	–	12.80	–	51.00	84
$CaLu_2Mg_2Si_3O_{12}$:0.005Cr^{3+}	SSR	1400	3	445	650−900	–	–	20.00	–	82.00	85
$Ca_{3-x}Lu_xHf_2Al_{2+x}Si_{1-x}O_{12}$:0.08$Cr^{3+}$	SSR	1600	4	460	700−1000	–	–	–	–	–	86
$CuSi_4O_{10}$:0.5Ca,0.5Sr	SSR	1050	10	620	700−1300			35.30		70.00	87
$Ca_8Mg(SiO_4)_4Cl_2$:Eu^{2+},Er^{3+}	SSR	1100	2	378	500−1600	RET	–	–	–	–	88
$Mg_2Al_4Si_5O_{18}$:0.02Cr^{3+}	SSR	1430	6	453	650−1200	–	NNI	–	–	>45.20	89
$Mg_2Al_4Si_5O_{18}$:Eu^{2+},0.01Cr^{3+}	SSR	1500	4	460	700−1200	–	–	–	55.48	∼38.00	90
$NaY_9Si_6O_{26}$:0.1Yb^{3+}	SSR	1400	8	270	950−1100	–	–	–	–	98.00	91
Eu, Yb doped silicate glass ($74SiO_2$−$10CaO$−$16Na_2O$)	SSR	1500	3	325	350−1150	CET	–	–	–	–	92

$$R_c \sim 2\left(\frac{3v}{4\pi X_c N}\right)^{1/3} \quad (1)$$

where N is the number of sites in the unit cell, i.e., possible occupancy of the activator ion. The value of π is 3.14. X_c is the optimized concentration of the activator ion, and v is the volume of the unit cell. To further discuss the specific mechanism, according to Dexter's theory,[38−40] the interaction type could be estimated using the following equation.

$$\log\left(\frac{I}{c}\right) = x - \frac{\theta}{3}\log(c) \quad (2)$$

where I and c represent the maximum intensity and concentration for individual phosphors. Here, x is constant. The electric multipolar character (θ) value is found from the linear graph between $\log(I/c)$ and $\log(c)$, when θ = 6, 8, and 10 corresponds to dipole−dipole (DDI), dipole−quadrupole (DQI), and quadrupole−quadrupole (QQI) interactions, respectively. If the θ value is closer to 3, it reveals that the concentration quenching resulted from nearby ionic interaction (NNI).[41]

3. SYNTHESIS STRATEGY OF NIR SILICATE PHOSPHOR

Commonly, the methods used to develop silicate phosphors are the solid-state method, coprecipitation, sol−gel, hydrothermal, etc. Sol−gel is one of the methods used to synthesize the phosphor at low temperatures. The precursors are taken and dissolved in an alcoholic medium to form the sol. Then, the sol undergoes the gelation process to form a gel. The gel is allowed to be dried and calcined to form a phosphor. Though the method is cost-effective and offers a low synthesis temperature, it lacks from regulation of particle size and aggregation/agglomeration of the particle.[42−45]

Hydrothermal is the chemical method used to synthesize the phosphor in the presence of high pressure and temperature. The

https://doi.org/10.1021/acsomega.3c08806
ACS Omega 2024, 9, 16880−16892

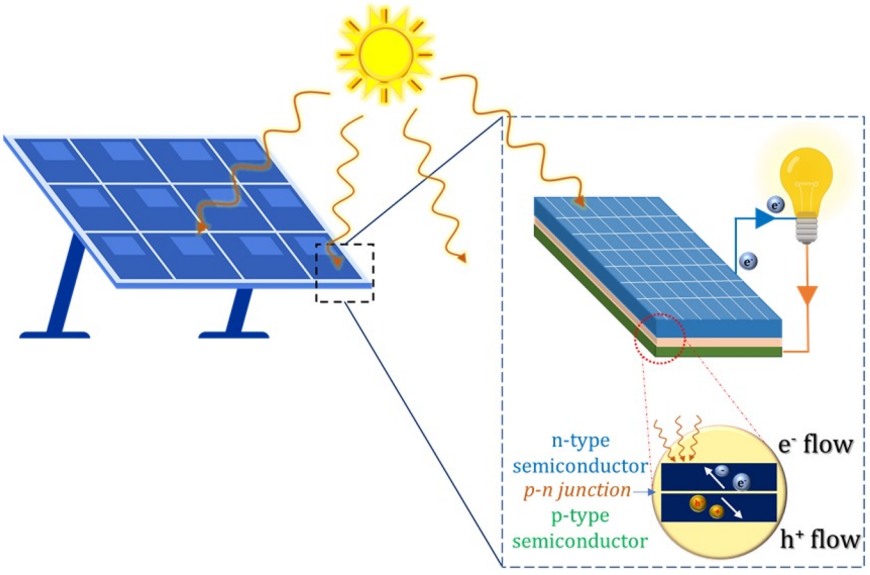

Figure 2. Schematic representation of working principle of solar cell.

precursor is taken in the form of salts in an aqueous/alcohol medium. Then, the solution is transferred into an autoclave at high temperatures and pressure. Hydrolysis followed by the condensation process results in the development of phosphor. This method increases the solubility of starting materials and also involves controlled growth of crystals.[46−49] However, this method often requires high pressure and temperature because of its limitations.

Coprecipitation is another way to synthesize the phosphor by adding precipitating agents like ammonium or sodium hydroxide to the precursor solution. This method is simple and does not require complex equipment. However, controlling the particle size is difficult.[50−52]

However, the NIR-emitting silicate phosphor shown in Table 1 is generally the preferred high-temperature solid-state reaction (SSR) technique as a synthesis strategy. Solid-state phosphor synthesis is a well-known conventional approach. To incorporate the activator ions into the host matrixes, the powdered raw materials are heated above their melting points. The advantages of this process include obtaining homogeneous mixing of metal ions at the molecular level, obtaining extremely tiny particles with a high packing density, and offering better crystalline structures with high purity.[53−57]

4. UNTIL NOW, NIR EMITTING SILICATE PHOSPHORS

According to the literature review, phosphor improves solar cell efficiency by being employed in solar cell applications. Because the solar cell is concentrated between 900 and 1100 nm, NIR-emitting silicate phosphors play a crucial role.[58] The silicate phosphors are involved in downconversion or downshifting, which includes emitting one or two NIR photons. As a result, the application of silicate phosphor fits the incident solar spectrum and the spectral response of solar cells, resulting in greater cell efficiency. The ideal host material should have low lattice photon energies to suppress nonradiative losses and a highly crystalline structure with minimal lattice defects and impurities.[59] The silicate phosphor is extremely heat stable and provides excellent quantum yield, tunable band gap, water resistance, high melting temperature, and rigid crystal structure, among other host matrixes, making it a good option for solar cell applications. Table 1 shows the unexplored silicate phosphor (PSR) with NIR emission in the solar application that has so far been developed. The synthesis strategy (SS) including the process temperature (T) and time (t), maximum excitation wavelength (λ_{ex}), and emission wavelength (λ_{em}) of the phosphor is given. The energy transfer process (ET) including the specific mechanism (SM) and energy transfer percentage between the activator and sensitizer (%ET) also discussed. In addition, the thermal stability of the phosphor up to 150 °C of that of room temperature ($I_{150\,°C}$ (%)) and internal quantum efficiency (IQE) are also given in Table 1.

Solar cells are typically most efficient at converting sunlight in a narrow wavelength range (900−1100 nm). However, solar cells frequently do not convert photons in the near-infrared region efficiently. NIR phosphors can be used to extend the solar cell's effective absorption spectrum, allowing it to capture more of the available sunlight. During the absorption process, high-energy photons may lose some of their energy as heat.[93] Some of these high-energy photons can be converted into lower-energy photons that the solar cell can absorb more efficiently by employing NIR silicate phosphors, lowering thermalization losses and boosting overall efficiency. Furthermore, NIR silicate phosphors are discussed in Table 1 and showed high thermal stability up to 150 °C. In addition, the high-temperature solid-state reaction method proves the high crystal purity, leading to the proper distribution of cations and action ions in the host crystal matrix, resulting in high quantum efficiency. This quality proves them ideal for long-term use in solar cell applications. The use of NIR silicate phosphors will enhance and sustain the performance of solar cells over long periods of time, particularly in outdoor situations where they are subjected to variable weather conditions.

5. WORKING PRINCIPLE AND PARAMETERS OF SOLAR CELL

Solar cells, also known as photovoltaic cells, are devices that convert sunlight into electricity via the photovoltaic effect. When sunlight reaches the surface of a solar cell, it generates charge carriers such as electrons and holes. The junction's internal field separates some positive charges (holes) from

https://doi.org/10.1021/acsomega.3c08806
ACS Omega 2024, 9, 16880−16892

Table 2. Solar Cell with Increase in Its Efficiency by Use of Silicate Phosphor

PSR	J_{SC} (mA/cm^2)	V_{OC} (mV)	FF (%)	η (%)	ΔJ_{SC} (%)	$\Delta\eta$ (%)	type	ref
$Ba_2SiO_4:Eu^{2+}/SiO_2$/Ag nanoparticle	42.04	600.00	68.00	17.77	–	–	c-Si	96
$SiO_2/[(Sr_{0.7}Ba_{0.3})_{0.98}Eu_{0.02}]_2SiO_{3.9}F_{0.1}$	32.02	534.35	77.28	13.22	30.27	36.57	c-Si	97
SiO_2/two phosphor (O, Si, Ba, Ti, Cl, Eu, Mn; and Sr, Si, Ba, Ti, Eu) layer	31.99	532.80	–	12.56	14.78	10.46	c-Si	98
SiO_2/two phosphor (O, Si, Ba, Ti, Cl, Eu, Mn; and Sr, O, Si, Ba, Eu, Mn) layer	33.09	534.40	–	12.49	19.85	15.97	c-Si	98
SiO_2/two phosphor (Sr, Si, Ba, Ti, Eu, Mn; and Sr, O, Si, Ba, Eu, Mn) layer	31.07	534.90	–	12.32	14.73	10.00	c-Si	98
SiO_2/two phosphor (O, Si, Ba, Ti, Cl, Eu, Mn; and Sr, Si, Ba, Ti, Eu) layer	31.61	535.50	75.50	12.77	13.58	14.02	c-Si	99
SiO_2/two phosphor (O, Si, Ba, Ti, Cl, Eu, Mn; and Sr, O, Si, Ba, Eu, Mn) layer	31.36	544.30	76.50	13.07	15.81	16.49	c-Si	99
SiO_2/two phosphor (Sr, Si, Ba, Ti, Eu, Mn; and Sr, O, Si, Ba, Eu, Mn) layer	31.83	545.80	76.40	13.26	19.39	19.35	c-Si	99
$SiO_2/(Sr_{1-x}Ba_x)_2SiO_4:Eu^{2+}F$ large phosphor particle	32.05	556.98	72.51	12.98	–	–	c-Si	100
$SiO_2/(Sr_{1-x}Ba_x)_2SiO_4:Eu^{2+}F$ medium phosphor particle	32.83	559.34	72.75	13.36	–	–	c-Si	100
$SiO_2/(Sr_{1-x}Ba_x)_2SiO_4:Eu^{2+}F$ small phosphor particle	33.43	560.77	73.94	13.86	–	–	c-Si	100
ITO/SiO_2−phosphor A (O, Si, Ba, Ti, Cl, Eu, and Mn)[a]	26.66	1053.00	82.63	23.20	20.14	19.83	GaAs	101
ITO/SiO_2−phosphor B (O, Sr, Si, Ba, Ti, Eu, and Mn)	26.72	1053.00	82.76	23.29	20.41	20.29	GaAs	101
ITO/SiO_2−phosphor C (Sr, O, Si, Ba, Eu, and Mn)	26.89	1053.00	82.77	23.44	21.18	21.07	GaAs	101
5% Eu-doped concave pyramidal microstructure silicate glass (Na_2CO_3:$CaCO_3$:SiO_2:CaF_2:Eu_2O_3)	37.11	615.00	66.32	14.61	–	0.41	c-Si	102
1.5Tb^{3+}−2Yb^{3+} doped silicate glass (72SiO_2−13.5Na_2O−10CaO−3.5MgO−0.5Al_2O_3−0.2Sb_2O_3−0.3 SnO_2)	39.36	627.00	77.80	19.20	–	–	c-Si	103
TiO_2/FTO/($K_2HfSiO_5:Eu^{2+}$ + polyvinylpyrrolidine) layer[b]	20.05	1012.00	72.48	16.73	–	2.19	$CsPbI_3$	104
Na_2CaSiO_4:5 mol % Ce^{3+},0.5 mol % Eu^{2+}	–	–	–	–	–	16.48	c-Si	105
PDMS + $(Ba,Ca,Eu,Sr)_2SiO_4$ + SiO_2 nanoparticle composite film[c]	16.74	1750.00	80.21	23.50	–	–	perovskite/silicon tandem	106
SiO_2/Ag nanoparticles/Eu-doped silicate phosphors in silicate glass solution	32.91	527.52	74.26	12.89	25.32	26.00	c-Si	107
Ag nanoparticles embedded in SiO_2 antireflective coating comprised Eu-doped phosphor (O, Si, Ba, Ti, Cl, Eu, and Mn)	32.85	549.74	79.02	14.27	–	26.17	c-Si	108
PDMS/$(Ba,Sr)SiO_4$:Eu	21.66	1010.00	75.58	16.51	22.80	25.30	GaAs	109
$SiO_2/(Sr_{1-x}Ba_x)_2SiO_4:Eu^{2+}F$ phosphor	29.55	–	–	34.33	11.52	15.38	c-Si	110
$SiO_2/(Sr_{1-x}Ba_x)_2SiO_4:Eu^{2+}F$ phosphor + SiO_2	31.18	545.50	78.20	13.35	19.42	19.70	c-Si	111
FTO/$TiO_2/(Sr,Ba,Eu)_2SiO_4$−TiO_2 composite layer	9.66	823.00	71.96	5.72	–	23.34	DSSC TiO_2	112
$Sr_3SiO_5:Ce^{3+},Al^{3+},Nd^{3+}$	–	–	–	–	7.70	–	–	65
SiO_2/3-silicate phosphor (O, Si, Ba, Ti, and Nb; O, Sr, Si, Ba, Ti, Nb with trace amounts of Mn and Eu; O, Sr, Si, Ba, Ti, Nb with trace amounts of Mn and Eu) (0.5:1:1.5)	28.92	524.70	73.05	11.08	18.81	20.43	c-Si	113
SiO_2 + $((Sr_{0.9}Ba_{0.1})_3SiO_5:Eu)$ + $[(Sr_{0.05}Ba_{0.95})_{0.98}Eu_{0.02}]SiO_{3.9}F_{0.1}$ layer	34.69	547.40	77.19	14.66	28.91	31.63	c-Si	114
$Y_2SrAl_4SiO_{12}$:0.05Ce^{3+},0.03Cr^{3+}	6.71	2419.00	75.38	12.24	–	2.02	c-Si	67

[a]ITO, indium tin oxide. [b]FTO, fluorine-doped tin oxide coated glass. [c]PDMS, polydimethylsiloxane.

negative charges (electrons). Holes are swept into the positive or p-layer, and electrons into the negative or n-layer. When a circuit is built, free electrons must pass through the load to recombine with positive holes; current can be generated from the cells when illuminated[94] as shown in Figure 2.

Several criteria are commonly used to characterize the performance of solar cells. Here are some crucial parameters:

Short circuit current (I_{SC}) is the maximum current produced by a solar cell and is often measured in amperes (A) or milliamperes (mA). When the cell is producing the maximum current (I_{SC} = 0.65 A), the open-circuit voltage is zero. The value of a short circuit is determined by the cell area, solar radiation on the cell, and cell technology. The short circuit current (I_{SC}) is the short circuit density (J_{SC}). ΔJ_{SC} defines the enhanced short circuit density.

The maximum voltage (V_{OC}) produced by a solar cell under an open circuit is known as the open circuit voltage. It is usually measured in volts (V) or millivolts (mV). When the cell produces maximum voltage, the short circuit current is equal to zero. The value of V_{OC} is determined by the cell technology and operating temperature. V_{OC} is the forward bias voltage at which the photocurrent density is compensated by the dark current density.

The fill factor (FF) represents the $I-V$ curve's squareness. It is the ratio of maximum power to the product of V_{OC} with J_{SC}. It is expressed as a percentage (%); the higher the fill factor in percent, the better the cell.

The product of voltage (V) and current (I) yields the maximum power point (PM). At the standard test condition, the maximum power point represents the maximum power that a solar cell can produce. The cell can function at various current and voltage combinations. However, it can only generate maximum power at a specific voltage and current combination.

The conversion efficiency (η) is calculated by dividing the maximum output power by the incident power. It is expressed as a percentage (%), indicating the highest proportion of input sunlight power that is converted to electrical power.[95] $\Delta\eta$ defines the enhanced conversion efficiency.

6. ROLE OF SILICATE PHOSPHOR IN SOLAR CELL

The solar conversion efficiency of a silicate phosphor is discussed in detail based on its particle size, coverage, volume concentration, arrangement, and so on. The type of silicate phosphor used and its enhancement of power conversion efficiency in solar cell applications are discussed in Table 2.

6.1. Influence of Particle Size. According to the Mie theory, the forward light scattering depends on the size of the particles. The larger the particles are, the larger the forward light scattering cross section, which results in higher conversion efficiency. Here the demonstrations are the following:

https://doi.org/10.1021/acsomega.3c08806
ACS Omega 2024, 9, 16880−16892

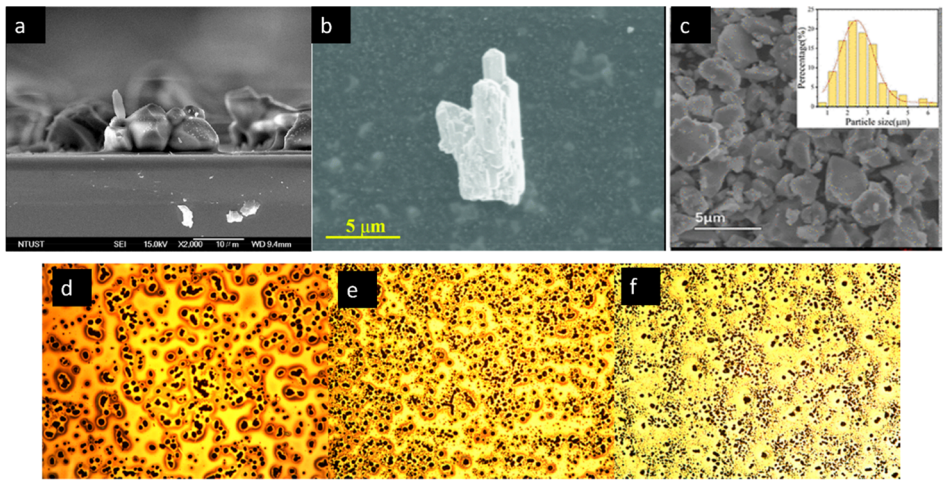

Figure 3. SEM images of $[(Sr_{0.7}Ba_{0.3})_{0.98}Eu_{0.02}]_2SiO_{3.9}F_{0.1}$ (a), $K_2HfSiO_5:Eu^{2+}$ (b), and $Y_2SrAl_4SiO_{12}:0.05Ce^{3+},0.03Cr^{3+}$ phosphor (c), and optical images of large, medium, and small phosphor particles (d, e, and f).[67,97,100,104] Reprinted from ref 67. Copyright 2023 American Chemical Society. Reprinted with permission from ref 97. Copyright 2016 Elsevier. Reprinted with permission from ref 104. Copyright 2022 Royal Society of Chemistry. From ref 100. CC BY 4.0.

By coating the SiO_2 with a phosphor layer over the bare cell, the conversion effectiveness is enhanced. Compared to the bare solar cell, Ho et al.[97] achieved J_{SC} increases of 15.01% (from 24.58 to 28.27 mA/cm^2) and 30.27% (from 24.58 to 32.02 mA/cm^2) for cells coated with SiO_2 layer and mixed layer of SiO_2−phosphor particles, respectively. The conversion efficacy of the cell coated with a SiO_2−phosphor layer is 13.22% greater than that of a bare solar cell (9.68%).[97] Figure 3a shows the phosphor particle size of 10−15 μm in diameter, and the coverage of the particle is found to be 7.64%. The work suggests that the phosphor particles absorb the photon in the range between 300 and 470 nm and results in the emission wavelength from 480 to 610 nm. The emitted photons are easily absorbed by the depletion region of the p−n junction, due to more charge carriers in the depletion region leading to higher photocurrent. Additionally, the enhanced external quantum efficiency obtained at wavelengths between 470 and 600 nm and beyond 600 nm is attributed to the antireflective property and forward light scattering property of the mixed layer of SiO_2−microscale phosphor.

Li et al.[104] developed a $K_2HfSiO_5:Eu^{2+}$ phosphor using a high-temperature solid-state reaction method. Then the energy downshift (EDS) layer solution is prepared using polyvinylpyrrolidine and phosphor via a spin-coating method over $CsPbI_3$. The average particle size is found to be 2.51 μm (Figure 3b). The prepared EDS layer showed no agglomeration of phosphor particles and leads to increased conversion efficacy by up to 2.19% over bare $CsPbI_3$ solar cells because of the forward scattering effect.[104]

Using $Y_2SrAl_4SiO_{12}:0.05Ce^{3+},0.03Cr^{3+}$ phosphor, Ma et al.[67] developed an energy downconversion (EDC) film that exhibits emission in the range of 500−800 nm at an excitation wavelength of 460 nm. The particle size is found to be in the range of 1−5 μm, and it is uniformly dispersed in the film (Figure 3c). The developed EDC film enhanced the power conversion efficiency by 2.02%, due to the forward scattering.[67]

Ho et al.[100] also investigated and improved the conversion efficiency of the Eu-doped silicate phosphor regarding the size of the phosphor particle. The Eu-doped silicate phosphor with particle sizes of 16.47 μm (large particle), 8.49 μm (medium particle), and 3.66 μm (small particle) is taken along with SiO_2 and coated over bare Si cells separately. The SiO_2−small phosphor particle showed higher absolute efficiency of 13.86% with SiO_2−medium and −large phosphor particles of 13.36 and 12.98%. The optical images show the coverage of large, medium, and small phosphor particles (Figure 3d−f). The small phosphor particle with dense coverage has a more pronounced effect on luminescent downshifting and a slight shading of incident light than an aggregation of larger particles, resulting in better conversion efficiency.[100]

From these studies, it is evident that, apart from the particle size, the aggregation of particles also affects the light scattering results in lowering the conversion efficiency.

6.2. Influence of Phosphor Coverage. Phosphor coverage is the second parameter, which also influences luminescence downshifting or downconversion. Higher uniform phosphor coverage, leading to more forward scattering, results in higher conversion efficiency.

Yang et al.[110] reported the improved efficiency of crystalline silicon (c-Si) solar cells using the combination of downshifting $(Sr_{1-x}Ba_x)_2SiO_4:Eu^{2+}F$ phosphor and SiO_2 antireflective coating via the spin-on coating process. The phosphor particles are in the size range of 10−20 μm, and the coverage of the particles is 6.9%. The enhancements of J_{SC} by 29.55% (11.52%) and power conversion efficiency by 34.33% (15.38%) are found due to the phosphor particle downshifting and scattering effect compared to the reference cell.[110]

To enhance the efficiency, Yang et al.[111] investigated the effect of the deposition holding time of the $(Sr_{1-x}Ba_x)_2SiO_4:Eu^{2+}F$ phosphor−SiO_2 solution on the cell substrate via the spin-on film technique on cell performance. The conversion efficiencies are 13.10, 13.35, and 12.26% for phosphor deposition holding times of 0, 5, and 15 s. The phosphor with 5 s demonstrated an increased conversion efficiency from 11.16 to 13.35%. The phosphor particles are of the size 10−20 μm, and the coverage of the particle is 25.09%. The coverages of particles of 0 and 15 s deposition times are 9.95 and 63.17%. Though the 15 s deposition time has high coverage, due to the particle aggregation, it showed lesser conversion efficiency. The density of the phosphor particles is controlled by deposition holding time resulting in enhanced conversion efficiency.[111]

https://doi.org/10.1021/acsomega.3c08806
ACS Omega 2024, 9, 16880−16892

Ho et al.[99] improved the conversion efficiency by combining a SiO_2 layer with two phosphor species. The phosphors emitting at 512, 550, and 610 nm are made up of O, Si, Ba, Ti, Cl, Eu, and Mn; Sr, Si, Ba, Ti, Eu, and Mn; and Sr, O, Si, Ba, Eu, and Mn. The conversion efficiencies of cells with single phosphor (512, 550, and 610 nm) were studied and showed efficiencies of 11.69, 13.03, and 13.74%. Additionally, the conversion efficiency of cells with two phosphors was also studied. The cell coated with SiO_2−phosphors (512 and 610 nm) layer increased conversion efficiency by 19.35% to the cell coated with SiO_2−phosphors (512 and 550 nm) layer and SiO_2−phosphors (550 and 610 nm) layer by 14.02 and 16.49%, respectively. The phosphor coverages of 610 nm and combined with two phosphors (512 and 610 nm) are 12.15 and 11.75%. Though a single phosphor (610 nm) has a high coverage of phosphor, it might lead to aggregation of phosphor and result in shading of light. This study suggests that the use of two phosphors increases the luminescent downshifting process, leading to increased phosphor uniform coverage resulting in enhanced conversion efficiency.[99]

These findings demonstrated that the conversion efficiencies are affected by the coverage of silicate phosphor coating on the cell substrate.

6.3. Influence of Phosphor Concentration. The phosphor volume concentration is also a parameter that decides the solar cell conversion efficiency. If the phosphor volume concentration increases, it causes a backscattering effect resulting in less conversion efficiency.

Lee et al.[106] developed an antireflective coating (ARC) polymeric film by embedding $(Ba,Ca,Eu,Sr)_2SiO_4$ phosphor and SiO_2 nanoparticles in PDMS. First, the ARC film by varying the concentration of phosphor (0, 0.4, 0.8, 1.2, and 1.6%) is fabricated. The film with a phosphor concentration of 0.4% showed a higher conversion efficiency of 22.75% than those with concentrations of 0.8 (22.43%), 1.2 (22.19%), and 1.6% (21.85%). Figure 4 shows the reflectance spectra of phosphor

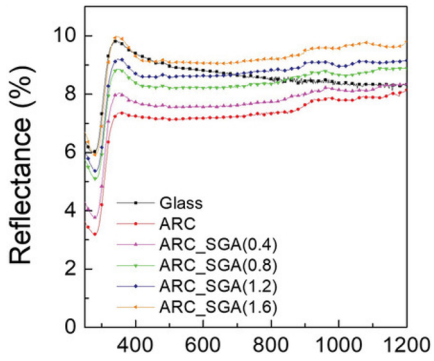

Figure 4. Reflectance spectra of phosphor with varying volume concentration. Reprinted with permission from ref 106. Copyright 2022 Wiley.

with varying concentrations. The 0.4% phosphor showed less reflectance than the other volume concentrations. However, the concentration of the phosphor decreases with increases in power conversion efficiency. The backscattering effect gets enhanced when the concentration of phosphor increases. If the particle size is larger than the wavelength of the incident light attributed to backward scattering, this might be because of aggregated particles. Then, SiO_2 nanoparticles are added to the ARC coating phosphor varying the volume of concentration, to compensate for the backscattering of phosphor particles via multiple scattering effects. This effect increases the conversion efficiencies of ARC film coating 0.8% phosphor and SiO_2 nanoparticle from 22.48 to 23.50% to the tandem solar cell.[106]

6.4. Influence of Phosphor Emission Wavelength. High-efficiency photovoltaic devices require a broad photoluminescence emission band and photon emissions at wavelengths in which the semiconductor has high responsivity. The responsivity value is directly proportional to the photogenerated current output at the same wavelength and incident light.

Ho et al.[101] increased the performance of GaAs cells with ITO/SiO_2/phosphor A, B, or C. The phosphors A, B, and C are made up of O, Si, Ba, Ti, Cl, Eu, and Mn; O, Sr, Si, Ba, Ti, Eu, and Mn; and Sr, O, Si, Ba, Eu, and Mn. The GaAs cells with ITO/SiO_2/phosphor C showed a lower reflectance and higher quantum efficiency of 14.11 and 72.62% than ITO/SiO_2/phosphor A (14.56, 72.11%) and B (14.46,72.47%). Based on the responsivity value of GaAs materials, Figure 5c clearly shows that the coating with ITO/SiO_2/phosphor C has a higher spectral match and it results in a conversion efficiency of 21.07% higher than that of the GaAs/ITO of 16.94%.[101]

Ho et al.[98] improved the conversion efficiency by spin coating SiO_2 with two distinct Eu-doped phosphor layers over the bare cell. The phosphors emitting at 512, 550, and 610 nm are made up of O, Si, Ba, Ti, Cl, Eu, and Mn; Sr, Si, Ba, Ti, Eu, and Mn; and Sr, O, Si, Ba, Eu, and Mn. The efficiencies of cells with a SiO_2 layer, cells with SiO_2−phosphors (512 and 550 nm), cells with SiO_2−phosphors (512 and 610 nm), and cells with SiO_2−phosphors (550 and 610 nm) are examined. Among these, the cell with phosphor combination (512 and 610 nm) demonstrated a 15.97% conversion efficiency due to the board band luminescent downshifting, forward scattering, and antireflection, compared with the cell with SiO_2 layer of 7.94%.[98]

Ho et al.[113] improved the performance of a c-Si solar cell by combining three kinds of Eu-doped silicate phosphor with SiO_2. Phosphor A is made up of O, Si, Ba, Ti, and Nb, as well as trace amounts of Eu, Mn, and Cl. Phosphors B and C are made up of O, Sr, Si, Ba, Ti, and Nb with trace amounts of Mn and Eu, and O, Sr, Si, Ba, Ti, and Nb with trace amounts of Mn and Eu. The maximum emission wavelengths for phosphors A, B, and C are 518.6, 551.3, and 609.1 nm, respectively. The three phosphor ratio structures: SiO_2 + 3-phosphor ratio (1.5:1:0.5), SiO_2 + 3-phosphor ratio (1:1:1), and SiO_2 + 3-phosphor ratio (0.5:1:1.5) have developed. The average reflectances and external quantum efficiencies were found to be 27.03, 26.79 and 26.63% and 59.76, 60.31, and 60.99%. The efficiency enhancement of the cell with a phosphor ratio of 0.5:1:1.5 wt % (20.43%) outperformed those of the cell with a phosphor ratio of 1:1:1 wt % (19.67%) and the cell with a phosphor ratio of 1.5:1:0.5 wt % (16.81%).[113]

Ho et al.[114] investigated the spectral conversion effect on c-Si solar cells with various combinations of Eu-doped silicate phosphor via a double coating method. The molar formula of phosphor E is $[(Sr_{0.05}Ba_{0.95})_{0.98}Eu_{0.02}]SiO_{3.9}F_{0.1}$, that of phosphor F is $[(Sr_{0.7}Ba_{0.3})_{0.98}Eu_{0.02}]_2SiO_{3.9}F_{0.1}$, and that of phosphor G is $(Sr_{0.9}Ba_{0.1})_3SiO_5$:Eu. The single coatings containing single phosphors such as SiO_2/phosphor E, SiO_2/phosphor F, and SiO_2/phosphor G showed efficiencies of 15.16, 16.08 and 17.39%. To enhance the efficiency, the three ratios of phosphor with SiO_2 were coated on solar cells such as SiO_2/phosphor E/phosphor F, SiO_2/phosphor F/phosphor G, and SiO_2/phosphor G/phosphor E. SiO_2/phosphor G/phosphor E showed an enhanced power conversion efficiency of 14.66% compared with those of SiO_2/phosphor E/phosphor F and

https://doi.org/10.1021/acsomega.3c08806
ACS Omega 2024, 9, 16880−16892

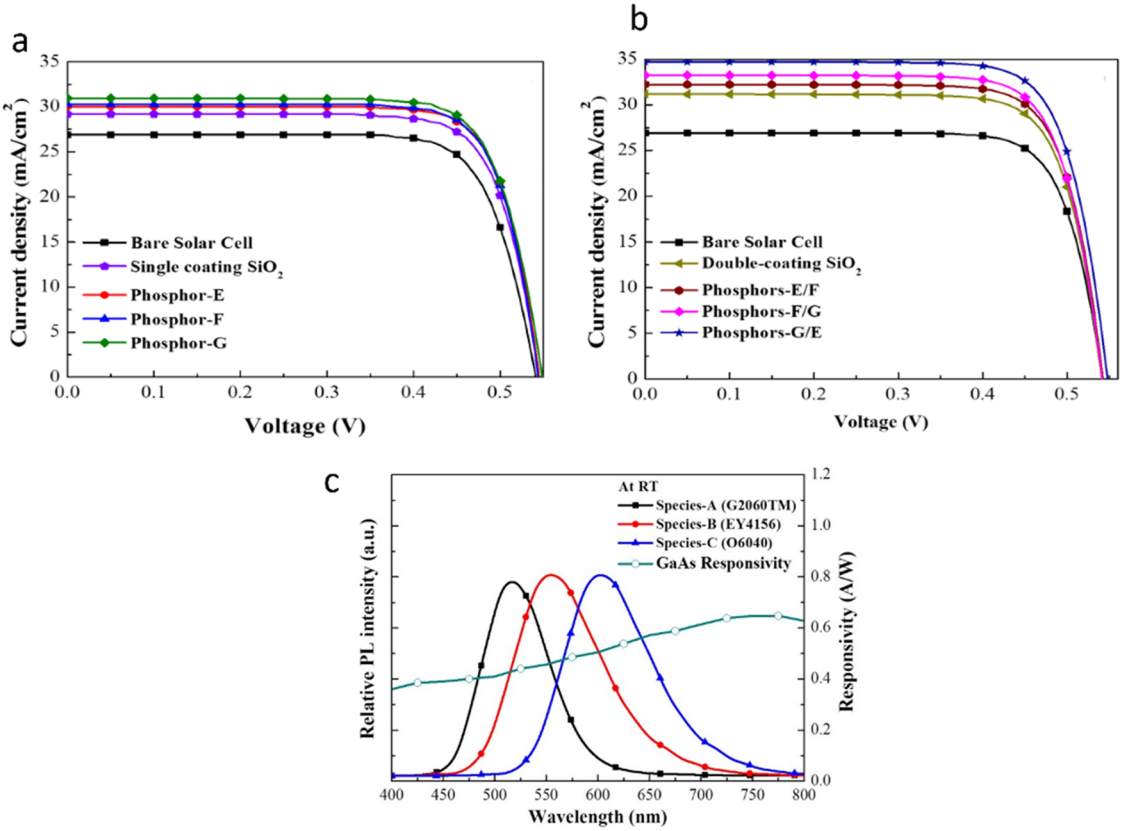

Figure 5. Photovoltaic $J-V$ curves of single phosphor (a) and double phosphor (b) and photoluminescence spectra of phosphors A/B/C (c).[101,114] Reprinted with permission from ref 101. Copyright 2018 Elsevier.

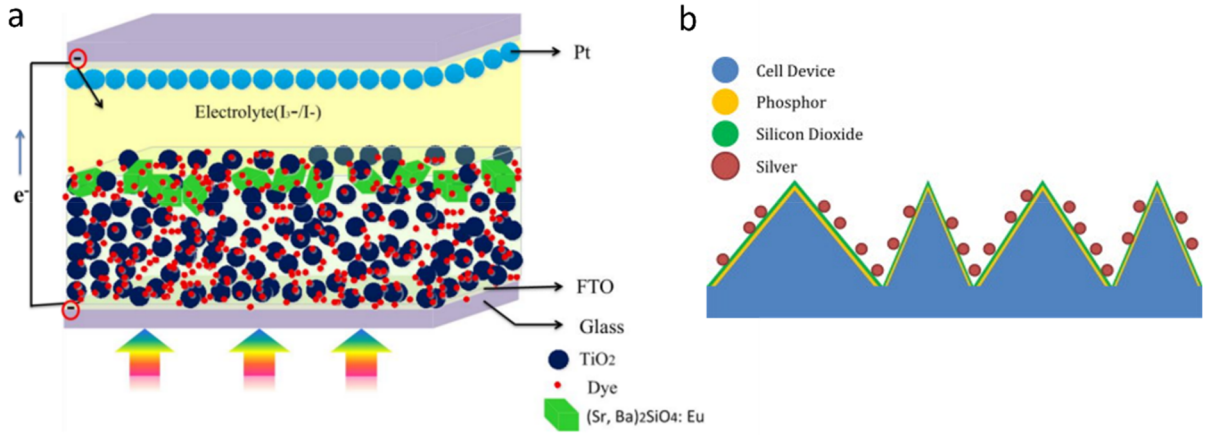

Figure 6. Structure of the solar cell with phosphor placement in the form of FTO/TiO_2/DC-TiO_2 (a) and Ba_2SiO_4:Eu^{2+}/SiO_2/Ag nanoparticle layers on microtextured c-Si solar cells (b). Reprinted with permission from ref 96. Copyright 2014 Elsevier. Reprinted with permission from ref 112. Copyright 2016 Elsevier.

SiO_2/phosphor F/phosphor G of 13.59 and 13.99%. The solar cell with SiO_2/phosphor G/phosphor E showed an enhanced efficiency of 31.63% over that of bare cells.[114] Figure 5b shows that the double coatings of SiO_2/phosphor G/phosphor E have higher current densities than a single phosphor with a single coating (Figure 5a), because of a low reflectance property. The combination of phosphors increased more pronounced effects on broadband luminescent downshifting emissions resulting in enhanced conversion than single coatings containing a single phosphor.

It is evident that, in reducing the reflectivity of photovoltaic devices, a larger number of incident photons enter the active layer of the photovoltaic devices to produce higher external quantum efficiency.

6.5. Influence of Phosphor Arrangement. The placement of the phosphor in solar cell devices also decides the change in conversion efficiency. For instance, Que et al.[112] developed three distinct structures and compared their solar cell parameters. FTO/TiO_2 (FTO, fluorine-doped tin oxide coated glass) is the first type, followed by FTO/DC-TiO_2/TiO_2 (DC, downconverting particle) and FTO/TiO_2/DC-TiO_2. When compared to types I and II, type III has higher J_{SC} (mA/cm^2), V_{OC} (mV), FF (%), and η (%) values of 9.66, 823, 71.96, and 5.72. The reason seems to be that some electrons may get

https://doi.org/10.1021/acsomega.3c08806
ACS Omega 2024, 9, 16880−16892

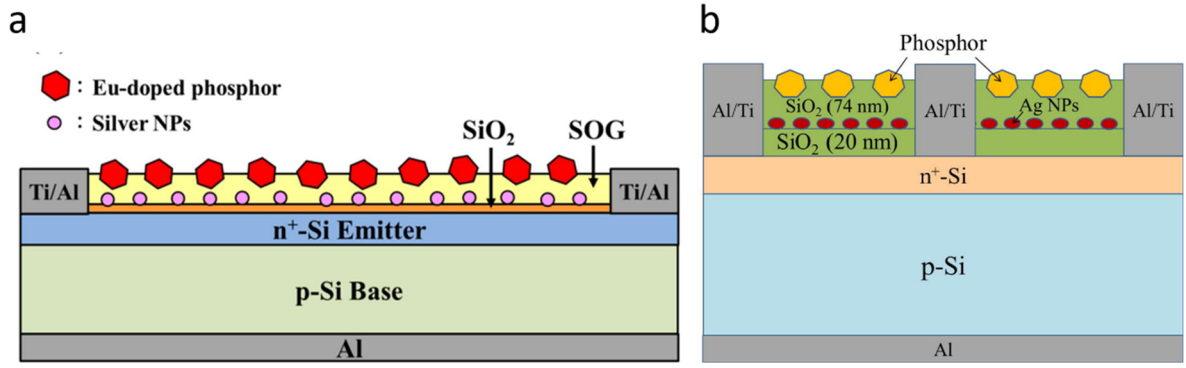

Figure 7. Structure of solar cell with phosphor and Ag nanoparticles (a) and with phosphor and Ag nanoparticles embedded in SiO_2 ARC (b). Reprinted with permission from ref 107. Copyright 2020 Elsevier. Reprinted with permission from ref 108. Copyright 2018 Elsevier.

through the porous film and reach the surface of the phosphor particles. The phosphor particles would absorb violet photons, and convert them to emission, which can be absorbed by the dye. As a result, structure III shown in Figure 6a can generate more photogenerated electrons, resulting in higher conversion efficiency.[112]

Chen et al.[96] synthesized green-emitting $Ba_2SiO_4:Eu^{2+}$ nanophosphors with needle-like morphology. The developed nanophosphor showed wide UV absorption from 300 to 450 nm and exhibited a quantum efficiency of 40%. $Ba_2SiO_4:Eu^{2+}/SiO_2$/Ag nanoparticles layers are fabricated on microtextured c-Si solar cells. The solar cells are coated with nanophosphor in various concentrations (1, 2, and 3 mg/mL) via a spin coating method. The phosphor with a concentration of 2 mg/mL showed an enhanced conversion efficacy of 0.19% than bare cells. Then, the efficiency is increased by 0.7% when the solar cell is coated with Ag nanoparticles and a 20 nm SiO_2 spacer. The phosphor with Ag nanoparticle-assisted c-Si solar cells showed higher J_{SC} (mA/cm^2) and η (%) values of 42.04 and 17.77 than bare solar cells of 41.18 and 17.06.[96] The thermally efficient $Ba_2SiO_4:Eu^{2+}$ phosphor functioned as luminescence down-shifting centers in the ultraviolet area, while the Ag nanoparticles aided in the enhancement of fluorescence in the visible range, increasing light absorption within the measured spectral regime. The enhancement of efficiency is mainly due to the placement of the phosphor on the front side (Figure 6b), which absorbs more photons closer to the depletion layer and involves in more conversion of UV photons to visible photons. The sensitivity of the cell at the incident light angle is reduced when the surface roughness of the cell increases after the phosphor deposition. Thus, the photons that reach the Ba_2SiO_4–air interface have more chances to be trapped in the cell and are involved in the generation of photocurrents around large incident angles.

6.6. Influence of Plasmonic Nanoparticles. Plasmonic metal (Ag) nanoparticles have been used with phosphor leading to a plasmonic forward scattering/plasmon-enhanced fluorescence effect, resulting in increased photovoltaic performance.

Ho et al.[107] enhanced the efficiency of solar cells using luminescent downshifting of Eu-doped phosphors and plasmonic Ag nanoparticles. The cell structure is prepared by depositing SiO_2 on bare cells through E-beam evaporation. Then a 3 nm thick Ag film is deposited over SiO_2 and followed by deposition of silicate glass solution containing phosphor as shown in Figure 7a. The enhanced J_{SC}, V_{OC}, FF, and η values from 26.26, 517.66, 75.27, and 10.23 of bare cells to 32.91, 527.52, 74.26, and 12.89 of the cells coated with SiO_2/Ag nanoparticles/Eu-doped silicate phosphor in silicate glass are noted. The increased conversion efficiency from 10.23 to 12.89% is observed for the silicate glass layer containing phosphor and Ag nanoparticles, across the wavelengths (380–1100 nm) and can be attributed to the plasmonic absorption and scattering of Ag nanoparticles as well as the antireflective effects of SiO_2 and phosphor.[107]

Ho et al.[108] improved the efficiency by including Eu-doped phosphor in a solar cell with a 3 mm thick film of Ag nanoparticles embedded in a SiO_2 ARC (Figure 7b). When compared to a bare cell, the addition of Ag nanoparticles and Eu-doped silicate phosphor increases conversion efficiency as follows: cell with SiO_2 ARC, 17.33% (from 11.31 to 13.27%); cell with Ag nanoparticles embedded in SiO_2 ARC, 22.63% (from 13.27 to 13.87%); and cell with Ag nanoparticles embedded in SiO_2 ARC comprised of Eu-doped silicate phosphor, 26.17% (from 13.87 to 14.27%). The luminous downshifting effect of Eu-doped silicate phosphor and the plasmonic scattering effect of Ag nanoparticles increased the power conversion efficiency by up to 26.17%.[108]

By comparing these two studies, solar cells with phosphor and Ag nanoparticles embedded in SiO_2 showed conversion efficiencies from 11.31 to 14.27% and SiO_2/Ag nanoparticles/Eu-doped silicate phosphor in silicate glass showed conversion efficiencies from 10.23 to 12.89%. Ag nanoparticles embedded showed better conversion efficiency, leading to a red shift resulting in an enhanced plasmonic forward scattering effect.

6.7. Influence of Dopant on Silicate Glass. Silicate glass is transparent to UV and possesses high chemical, thermal, and mechanical stabilities. The photovoltaic glass can act as a downconversion carrier.

To enhance the downconversion efficiency of the silicate glass, Yang et al.[102] studied and compared the conversion efficiencies of Eu^{3+}-doped silicate glass, undoped silicate glass, and Eu^{3+}-doped glass embedded with a concave pyramidal microstructure. The Eu^{3+}-doped silicate glass was prepared by a solid-state reaction technique with a molar ratio of $Na_2CO_3:CaCO_3:SiO_2:CaF_2:Eu_2O_3$ = 1:1:6:1:5. Eu-doped glass showed a conversion efficacy of 14.10% due to the light scattering effect. To further increase efficiency, Eu-doped glass with a micropyramid structure was developed using the specific mold and showed 14.61%. The micropyramid structure increases light transmission and results in increased efficiency, as shown in Figure 8.[102]

Similar work is found by Zhao et al.,[103] who developed different ratios of Tb^{3+}- and Yb^{3+}-doped silicate glass as a downconversion layer and studied their conversion efficiency. The Tb^{3+},Yb^{3+}-doped silicate glasses were prepared via the solid

https://doi.org/10.1021/acsomega.3c08806
ACS Omega 2024, 9, 16880−16892

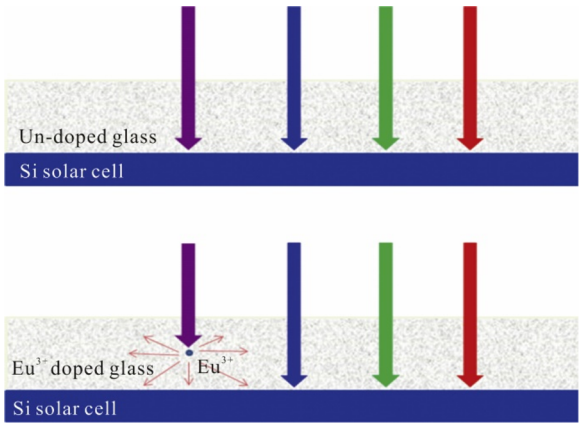

Figure 8. Light scattering effect of Eu^{3+}-doped silicate glass. Reprinted with permission from ref 102. Copyright 2020.

phase high-temperature method with a composition of $72SiO_2-13.5Na_2O-10CaO-3.5MgO-0.5Al_2O_3-0.2Sb_2O_3-0.3SnO_2-xTb^{3+}-yYb^{3+}$ (x = 0, 1.5 and y = 0, 1.5, 2, 3 mol %). The cell with $1.5Tb^{3+}-2Yb^{3+}$ glass showed a higher conversion efficacy of 19.20% than the cell with $1.5Tb^{3+}-1.5Yb^{3+}$and $1.5Tb^{3+}-3Yb^{3+}$ glasses of 18.56 and 18.33%, respectively. The efficiency of a solar cell with $1.5Tb^{3+}-2Yb^{3+}$ glass increased by up to 8.6% than a cell without glass by 17.68%.[103] The incorporation of dopants (Tb^{3+}, Yb^{3+}) into glass material demonstrates a high adsorption capacity in the solar cell spectral region via a downconversion mechanism.

The glasses are highly thermally stable. These experiments suggest that the incorporation of dopant or phosphor into the glass tends to reduce thermal loss, resulting in higher conversion efficiency.

7. CONCLUSION AND PROSPECTS

The addition of phosphor improved the power conversion efficiency of a bare solar cell. The influences of size, amount, coverage, volume concentration, emission wavelength, and placement of phosphor on energy conversion are explained in detail. The energy transfer mechanism of lanthanide ions in NIR silicate phosphor, the so-far developed NIR silicate phosphor, the synthesis process, and the use of silicate phosphor in boosting the power conversion efficiency of solar cells are examined in this review. The following are some promising paths for developing new silicate phosphors to improve solar cell efficiency:

1. Multicolor silicate phosphors: Developing silicate phosphors that emit light in a variety of colors or wavelengths can be useful for harnessing a greater range of solar energy. In multijunction solar cells, these multicolor phosphors can be tuned to fit the absorption characteristics of various semiconductor materials.

2. Core−shell nanoparticles: In silicate phosphors, using core−shell nanoparticles can improve their stability and emission qualities. Researchers can manage emission characteristics and energy conversion efficiency by constructing the core and shell materials accordingly.

3. Quantum dot enhanced phosphors: By combining silicate phosphors with semiconductor quantum dots, new materials with precisely controllable emission properties can be created. Quantum dots can be used as sensitizers to boost the performance of silicate phosphors.

4. Perovskite−silicate hybrid phosphors: Due to their remarkable absorption properties, perovskite materials have shown tremendous promise in solar cells. Developing hybrid phosphors with silicate and perovskite materials can boost light absorption and energy conversion.

5. Plasmonic silicate phosphors: Metallic nanoparticles such as Ag, Au, etc. can improve light absorption. Silicate phosphors with plasmonic characteristics can absorb more energy from the solar spectrum, particularly in the visible and near-infrared ranges.

6. Porous silicate phosphor: The silicate phosphor with a porous structure has a higher surface area, resulting in higher absorption of solar light, which leads to higher power conversion efficiency.

7. Ultrastable phosphors: Developing silicate phosphors with remarkable long-term stability can help solar cells last longer and maintain high efficiency over time, lowering maintenance and replacement costs.

In this way, we can achieve a higher power conversion efficiency in the future.

AUTHOR INFORMATION

Corresponding Author

Abinaya Mayavan − *School of Chemistry, University of Hyderabad, Hyderabad 500046 Telangana, India;* orcid.org/0000-0002-9377-9433; Phone: +91-8220077256; Email: abinaya_i_pdrf@uohyd.ac.in

Complete contact information is available at: https://pubs.acs.org/10.1021/acsomega.3c08806

Notes

The author declares no competing financial interest.

ACKNOWLEDGMENTS

The author thanks University of Hyderabad, Telangana, for providing Institute of Eminence (IoE) funds and infrastructural support. Also, the author expresses sincere gratitude to Harikrishnan Venkatesvaran, National Taipei University of Technology, Taiwan, for sketching the graphical abstract.

REFERENCES

(1) Raha, S.; Pal, S. A study on the present environmental scenario due to pollution by conventional energy sources-and remedies. *Strategic Planning for Energy and the Environment* **2010**, *30*, 8−19.

(2) KhareSaxena, A.; Saxena, S.; Sudhakar, K. Solar energy policy of India: An overview. *CSEE Journal of Power and Energy Systems* **2020**, DOI: 10.17775/CSEEJPES.2020.03080.

(3) O'Regan, B.; Gratzel, M. A low-cost, high- efficiency solar cell based on dye- sensitized collidal TiO2 films. *Nature* **1991**, *353*, 737−740.

(4) Samuel, A. K.; Dileep K, R.; Jayaraman, M.; Veerappan, G.; Jayaraman, S. Enhanced Power Conversion Efficiency Using a Ce3+:SrF2Down-Shifting Nanophosphor-Based Photoelectrode for Dye-Sensitized Solar Cell Applications. *ACS Appl. Energy Mater.* **2021**, *4*, 7112−7121.

(5) Hora, C.; Santos, F.; Sales, M. G. F.; Ivanou, D.; Mendes, A. Dye-sensitized solar cells for efficient solar and artificial light conversion. *ACS Sustain Chem. Eng.* **2019**, *7*, 13464−70.

(6) Hendi, A. A.; Alanazi, M. M.; Alharbi, W.; Ali, T.; Awad, M. A.; Ortashi, K. M.; et al. Dye-sensitized solar cells constructed using titanium oxide nanoparticles and green dyes as photosensitizers. *J. King Saud Univ Sci.* **2023**, *35*, No. 102555.

(7) Chapin, D. M.; Fuller, C. S.; Pearson, G. L. A new silicon p−n junction photocell for converting solar radiation into electrical power [3]. *J. Appl. Phys.* **1954**, *25*, 676−7.
(8) Kim, S. H.; Jung, J. Y.; Wehrspohn, R. B.; Lee, J. H. All-Room-Temperature Processed 17.25%-Crystalline Silicon Solar Cell. *ACS Appl. Energy Mater.* **2020**, *3*, 3180−5.
(9) Welter, K.; Becker, J. P.; Finger, F.; Jaegermann, W.; Smirnov, V. Performance of Integrated Thin-Film Silicon Solar Cell-Based Water-Splitting Devices under Varying Illumination Angles and an Estimation of Their Annual Hydrogen Production. *Energy Fuels* **2021**, *35*, 839−46.
(10) Daiber, B.; Van Den Hoven, K.; Futscher, M. H.; Ehrler, B. Realistic Efficiency Limits for Singlet-Fission Silicon Solar Cells. *ACS Energy Lett.* **2021**, *6* (8), 2800.
(11) Kojima, A.; Teshima, K.; Shirai, Y.; Miyasaka, T. Organometal halide perovskites as visible-light sensitizers for photovoltaic cells. *J. Am. Chem. Soc.* **2009**, *131*, 6050−1.
(12) Lee, C.; Chae, K.; Ko, Y.; Lee, C.; Kim, T.; Park, S.; et al. Phase Stability Improvement of a γ-CsPbI3 Perovskite Solar Cell Utilizing a Barium Bis(trifluoromethanesulfonimide) Solution. ACS Appl Mater. *Interface* **2023**, *15*, 51050−51058.
(13) Aeineh, N.; Barea, E. M.; Behjat, A.; Sharifi, N.; Mora-Seró, I. Inorganic Surface Engineering to Enhance Perovskite Solar Cell Efficiency. *ACS Appl. Mater. Interfaces* **2017**, *9*, 13181−7.
(14) Wang, J.; Zhang, H.; Wang, L.; Yang, K.; Cang, L.; Liu, X.; et al. Highly Stable and Efficient Mesoporous and Hollow Silica Antire-flection Coatings for Perovskite Solar Cells. *ACS Appl. Energy Mater.* **2020**, *3*, 4484−91.
(15) Gorter, T.; Reinders, A. H. M. E. A comparison of 15 polymers for application in photovoltaic modules in PV-powered boats. *Appl. Energy* **2012**, *92*, 286−297.
(16) Yang, C.; Sun, Y.; Li, Q.; Liu, K.; Xue, X.; Huang, Y.; et al. Nonfullerene Ternary Organic Solar Cell with Effective Charge Transfer between Two Acceptors. *J. Phys. Chem. Lett.* **2020**, *11*, 927−34.
(17) Nicolaidis, N. C.; Al-Mudhaffer, M. F.; Holdsworth, J. L.; Zhou, X.; Belcher, W. J.; Dastoor, P. C. Contribution of Fullerene Photocurrent Generation to Organic Solar Cell Performance. *J. Phys. Chem. C* **2019**, *123*, 11950−8.
(18) Mohitkar, A.; H, R.; Goel, S.; Jayanty, S. Efficient Standalone Flexible Small Molecule Organic Solar Cell Devices: Structure-Performance Relation Among Tetracyanoquinodimethane Derivatives. *ACS Omega* **2023**, *8*, 40836−40847.
(19) Bruton, T. M. General trends about photovoltaics based on crystalline silicon. *Sol. Energy Mater. Sol. Cells* **2002**, *72*, 3−10.
(20) Bünzli, J. C. G.; Chauvin, A. S. Lanthanides in solar energy conversion. *Handbook on the Physics and Chemistry of Rare Earths* **2014**, *44*, 169−281.
(21) Keil, J.; Silvia, J. S.; Kroupa, D. M.; Ferry, V. E. Optical Coupling Efficiency, Photon Loss, and Efficiency Estimates for c-Si PERC Modules Enhanced with Downconverting Films and Nanocomposites. *ACS Appl. Energy Mater.* **2023**, *6*, 10978−86.
(22) Nakamura, Y.; Iso, Y.; Isobe, T. Bandgap-Tuned CuInS2/ZnS Core/Shell Quantum Dots for a Luminescent Downshifting Layer in a Crystalline Silicon Solar Module. *ACS Appl. Nano Mater.* **2020**, *3*, 3417−26.
(23) Shockley, W.; Queisser, H. J. Detailed balance limit of efficiency of p−n junction solar cells. *J. Appl. Phys.* **1961**, *32*, 510−9.
(24) Zhang, J.; Huang, Y.; Gong, X.; Huang, J.; Lin, Y.; Chen, Y. Spectroscopic and energy transfer properties of NaTb(WO4)2 phosphor and crystal sensitized by Dy3+. *J. Lumin.* **2023**, *257*, 119754−61.
(25) Wu, M.; Chen, W.; Liu, S.; Sun, Y.; Huang, L.; Chen, G.; et al. Sensitizing effect of Nd3+ on Tb3+ activated ZrP2O7 long persistent phosphor materials. *Journal of Rare Earths* **2021**, *39*, 757−64.
(26) Nair, G. B.; Dhoble, S. J. Phosphor-converted LEDs. In *The Fundamentals and Applications of Light-Emitting Diodes*Elsevier: 2021; pp 87−126..
(27) Silver, J.; Withnall, R. Color Conversion Phosphors for LEDS. In *Luminescent Materials and Applications*; Kitai, A., Ed.; John Wiley & Sons: 2008; pp 76−109..
(28) Hong, C. K.; Ou, Z. Y.; Mandel, L. Measurement of Subpicosecond Time Intervals between Two Photons by Interference. *Phys. Rev. Lett.* **1987**, *59*, 2044−6.
(29) Goetzberger, A.; Greube, W. Solar energy conversion with fluorescent collectors. *Applied Physics* **1977**, *14*, 123−39.
(30) Auzel, F. Up-conversions in RE-doped Solids. *Springer Series in Materials Science* **2005**, *83*, 266−319.
(31) Trupke, T.; Green, M. A.; Würfel, P. Improving solar cell efficiencies by down-conversion of high-energy photons. *J. Appl. Phys.* **2002**, *92*, 1668−74.
(32) Wang, B.; Liu, Y.; Huang, Z.; Fang, M. Photoluminescence properties of a Ce3+ doped Sr3MgSi2O8 phosphor with good thermal stability. *RSC Adv.* **2018**, *8*, 15587−94.
(33) Nasir, S. S. B.; Tanaka, A.; Yoshiara, S.; Kato, A. Luminescence properties of Li2SrSiO4:Eu2+ silicate yellow phosphors with high thermal stability for high-power efficiency white LED application. *J. Lumin.* **2019**, *207*, 22−8.
(34) Dexter, D. L. A theory of sensitized luminescence in solids. *J. Chem. Phys.* **1953**, *21*, 836−50.
(35) Blasse, G. Energy transfer in oxidic phosphors. *Phys. Lett. A* **1968**, *28*, 444−5.
(36) Dutta, S.; Som, S.; Meena, M. L.; Chaurasiya, R.; Chen, T. M. Multisite-Occupancy-Driven Intense Narrow-Band Blue Emission from Sr5SiO4Cl6:Eu2+ Phosphor with Excellent Stability and Color Performance. *Inorg. Chem.* **2020**, *59*, 1928−39.
(37) Song, S.; Si, J.; Zhang, J.; Cai, G. Structure, tunable luminescence and energy transfer in Tb3+ and Eu3+ codoped Ba3InB9O18 phosphors. *RSC Adv.* **2019**, *9*, 1029−35.
(38) Dexter, D. L.; Schulman, J. H. Theory of concentration quenching in inorganic phosphors. *J. Chem. Phys.* **1954**, *22*, 1063−70.
(39) Ye, W.; Zhao, C.; Shen, X.; Ma, C.; Deng, Z.; Li, Y.; et al. High Quantum Yield Gd4.67Si3O13:Eu3+Red-Emitting Phosphor for Tunable White Light-Emitting Devices Driven by UV or Blue LED. *ACS Appl. Electron Mater.* **2021**, *3*, 1403−12.
(40) Wei, S.; Lyu, Z.; Lu, Z.; Luo, P.; Zhou, L.; Sun, D.; et al. Moderate Trap Engineering for Enhanced Thermal Stability and High Efficiency in a Bi3+-Doped Phosphor. *Chem. Mater.* **2023**, *35*, 7125−32.
(41) Cui, S.; Chen, G. Investigation of photoluminescence properties, quenching mechanism and thermal stability of the red-emitting phosphor based on Eu ions doped apatite host NaLa9(SiO4)6O2. *Mater. Res. Express* **2019**, *6*, 096201.
(42) Copeland, T. S.; Lee, B. I.; Qi, J.; Elrod, A. K. Synthesis and luminescent properties of Mn2+-doped zinc silicate phosphors by sol-gel methods. *J. Lumin.* **2002**, *97*, 168−73.
(43) Singh, V.; Bajaj, R.; Kaur, S.; Rao, A. S.; Singh, N. UVB emission from sol-gel derived Gd3+-doped CaLa4Si3O13 phosphor. *Optik (Stuttg)* **2021**, *242*, No. 167275.
(44) Kuriyan, N. S.; Sabeena, M. Luminescence studies of Eu3+ doped calcium magnesium silicate phosphor prepared at different annealing temperatures for fine color tunability. *J. Lumin.* **2022**, *249*, No. 119038.
(45) Kaur, H.; Jayasimhadri, M.; Sahu, M. K.; Rao, P. K.; Reddy, N. S. Synthesis of orange emitting Sm3+ doped sodium calcium silicate phosphor by sol-gel method for photonic device applications. *Ceram. Int.* **2020**, *46*, 26434−9.
(46) Zaitseva, N. A.; Krasnenko, T. I.; Onufrieva, T. A.; Samigullina, R. F. Hydrothermal synthesis and microstructure of α-Zn2SiO4:V crystal phosphor. *Russ. J. Inorg. Chem.* **2017**, *62*, 168−71.
(47) Yang, Y.; Pan, H.; Guan, L.; Wang, D.; Zhao, J.; Yang, J.; et al. Electronic structure and luminescent properties of Sr3Al2O6:Sm3+ orange phosphor prepared by hydrothermal method. *Journal of Materials Research and Technology* **2020**, *9*, 3847−55.
(48) Manaka, M. C.; Mothudi, B. M.; Dhlamini, M. S. Thermoluminescence properties of beta irradiated SrSiO3/SiO2 phosphor synthesized by hydrothermal method. *Physica B: Condens. Matter* **2023**, *671*, 415397.

https://doi.org/10.1021/acsomega.3c08806
ACS Omega 2024, 9, 16880−16892

(49) Diana, P.; Sebastian, S.; Sivaganesh, D.; Manthrammel, M. A.; Kumar, A.; Shkir, M. Hydrothermal synthesis of cerium-doped Zn2SiO4 phosphor for futuristic lighting applications. *J. Solid State Chem.* **2024**, *329*, No. 124441.
(50) Sahu, I. P. Orange-red emitting europium doped strontium ortho-silicate phosphor prepared by a solid state reaction method. *Luminescence* **2017**, *32*, 364−74.
(51) Chen, J.; Yang, Y.; Xu, J.; Mao, Z.; Wang, D.; Bie, L.; et al. High-temperature crystalline α'H- and α-Ca2SiO4:Eu2+ phosphors stabilized at room temperature by incorporating phosphorus ions. *RSC Adv.* **2016**, *6*, 83776−82.
(52) Yang, L.; Zhu, D.; Liu, S.; Wang, J.; Zhao, C.; Pu, Y. Photoluminescence properties and crystal structure of BaSiO3:xEu3+, yBi3+ red phosphor synthesized by co-precipitation method. *Physica B: Condens Matter* **2019**, *556*, 6−11.
(53) Balakrishnan, P.; Masilla Moses Kennedy, S. Tunable light emission from single phased Ba2CaZn2Si6O17:Pb2+, Eu3+ silicate phosphors via energy transfer efficiency for white light emitting diode applications. *Solid State Sci.* **2021**, *118*, No. 106665.
(54) Sahu, I. P.; Bisen, D. P.; Brahme, N. Europium doped di-calcium magnesium di-silicate orange−red emitting phosphor by solid state reaction method. *J. Radiat Res. Appl. Sci.* **2015**, *8*, 381−8.
(55) Kuriyan, N. S.; Ghosh, P. S.; Arya, A.; Sabeena, M. Site preference-based luminescence studies in Eu doped calcium magnesium silicate phosphor: A combined experimental and DFT approach. *J. Lumin.* **2023**, *260*, No. 119901.
(56) Wu, M.; Wei, H.; Huang, X.; Liu, Q.; Duan, S.; Liu, Y.; et al. High-Efficiency Ce3+ Activated Orthorhombic Lanthanide Silicate Blue Phosphors for Plant Growth Lighting. *Inorg. Chem.* **2023**, *62*, 12793−802.
(57) Lee, C. Y.; Wu, C. C.; Li, H. H.; Yang, C. F. Synthesis and Luminescence Properties of Eu2+-Doped Sr3MgSi2O8 Blue Light-Emitting Phosphor for Application in Near-Ultraviolet Excitable White Light-Emitting Diodes. *Nanomaterials* **2022**, *12*, 2706.
(58) Suresh, K.; Jayasankar, C. K. Spectral investigations of Sm3+/Yb3+: TeO2 + ZnO + Nb2O5 + TiO2 glasses for the conversion of Si -based solar cell applications. *J. Alloys Compd.* **2018**, *750*, 420−7.
(59) Abdelbar, M. F.; El-Kemary, M.; Fukata, N. Downshifting of highly energetic photons and energy transfer by Mn-doped perovskite CsPbCl3 nanocrystals in hybrid organic/silicon nanostructured solar cells. *Nano Energy* **2020**, *77*, No. 105163.
(60) Chen, J.; Guo, C.; Yang, Z.; Li, T.; Zhao, J. Li2SrSiO4: Ce3+, Pr3+ Phosphor with Blue Red and Near-Infrared Emissions Used for Plant Growth LED. *J. Am. Chem. Soc.* **2016**, *99*, 218−25.
(61) Wang, L.; Li, Y. F.; Wang, Z.; Yang, R.; Tong, Y.; Sun, L. Resonant energy transfer and near-infrared emission enhanced by tri-doped Sr2SiO4: Ce3+, Tb3+, Yb3+ phosphors for silicon solar cells. *J. Lumin.* **2018**, *203*, 121−6.
(62) Vyas, A.; Joshi, C. P.; Sahare, P. D.; Moharil, S. V. NIR emission in Ba2SiO4:Eu2+, Nd3+ phosphors with near UV/violet excitation. *J. Alloys Compd.* **2018**, *743*, 789−94.
(63) Nanai, Y.; Ishida, R.; Urabe, Y.; Nishimura, S.; Fuchi, S. Octave-spanning broad luminescence of Cr3+, Cr4+ -codoped Mg2SiO4 phosphor for ultra-wideband near-infrared LEDs. *Jpn. J. Appl. Phys.* **2019**, *58*, No. SFFD02.
(64) Wen, H.; Mo, Z.; Ta, C.; Mu, Z.; Dawi, E. A.; Sun, M.; et al. Improvement in the dual-mode multicolor luminescence of the NaAlSiO4:Er3+, Yb3+ phosphors and the mechanistic investigations. *J. Lumin.* **2023**, *254*, No. 119486.
(65) Chen, J.; Liu, J.; Yao, H.; Li, X.; Yao, Z.; Yue, H.; et al. Preparation and application of strong near-infrared emission phosphor Sr3SiO5:-Ce3+,Al3+,Nd3+. *J. Am. Ceram. Soc.* **2015**, *98*, 1836−41.
(66) Mao, M.; Zhou, T.; Zeng, H.; Wang, L.; Huang, F.; Tang, X.; et al. Broadband near-infrared (NIR) emission realized by the crystal-field engineering of Y3-xCaxAl5- xSixO12:Cr3+ (x = 0−2.0) garnet phosphors. *J. Mater. Chem. C Mater.* **2020**, *8*, 1981−8.
(67) Ma, X.; Seto, T.; Wang, Y. A Deep-Red Emission Phosphor Y2SrAl4SiO12:Ce3+, Cr3+ and Its Utilization in Polycrystalline Silicon Solar Cells. *J. Phys. Chem. Lett.* **2023**, *14*, 535−44.
(68) Hou, D.; Lin, H.; Zhang, Y.; Lin, Z.; Li, H.; Song, J.; et al. A novel extra-broadband visible-NIR phosphor doped with Ce3+ and Cr3+ towards multifunctional advanced applications. *Ceram. Int.* **2023**, *49*, 10692−701.
(69) Jiang, L.; Jiang, X.; Zhang, L.; Liu, Q.; Mi, X.; Yu, Z.; et al. Broadband Near-Infrared Luminescence in Garnet Y3Ga3MgSiO12: Cr3+ Phosphors. *Inorg. Chem.* **2023**, *62*, 4220−6.
(70) Ding, S.; Guo, H.; Feng, P.; Ye, Q.; Wang, Y. A New Near-Infrared Long Persistent Luminescence Material with Its Outstanding Persistent Luminescence Performance and Promising Multifunctional Application Prospects. *Adv. Opt Mater.* **2020**, *8*, 1−12.
(71) Xu, X.; Shao, Q.; Yao, L.; Dong, Y.; Jiang, J. Highly efficient and thermally stable Cr3+-activated silicate phosphors for broadband near-infrared LED applications. *Chemical Engineering Journal* **2020**, *383*, No. 123108.
(72) Yan, Y.; Shang, M.; Huang, S.; Wang, Y.; Sun, Y.; Dang, P.; et al. Photoluminescence Properties of AScSi2O6:Cr3+(A = Na and Li) Phosphors with High Efficiency and Thermal Stability for Near-Infrared Phosphor-Converted Light-Emitting Diode Light Sources. *ACS Appl. Mater. Interfaces* **2022**, *14*, 8179−90.
(73) Lu, Z.; Liu, Y.; Chen, S.; Sun, P.; Luo, Z.; Wang, X.-J.; et al. Improved Near-Infrared Luminescence Properties of LiScSi 2 O 6 :Cr 3+, Yb 3+ Phosphors via Efficient Energy Transfer. *ACS Applied Optical Materials* **2023**, *1*, 1097−103.
(74) Zhang, Q.; Wang, X.; Tang, Z.; Wang, Y. A K3ScSi2O7: Eu2+ based phosphor with broad-band NIR emission and robust thermal stability for NIR pc-LEDs. *Chem. Eng. Commun.* **2020**, *56*, 4644−4647.
(75) Talewar, R. A.; Mahamuda, S.; Vyas, A.; Rao, A. S.; Moharil, S. V. Enhancement of 1.54 μm emission in Ce3+-Er3+ codoped Ca4-Si2O7F2 phosphor. *J. Alloys Compd.* **2019**, *775*, 810−7.
(76) Dai, W. B.; Zhou, J.; Huang, K.; Hu, J.; Xu, S.; Xu, M. Investigation on structure and optical properties of down-conversion aluminosilicate phosphors CaAl2Si2O8: Ce/Tb/Yb. *J. Alloys Compd.* **2019**, *786*, 662−7.
(77) Jin, Y.; Zhou, Z.; Ran, R.; Tan, S.; Liu, Y.; Zheng, J.; et al. Broadband NIR Phosphor Ca2LuScAl2Si2O12:Cr3+ for NIR LED Applications. *Adv. Opt Mater.* **2022**, *10*, 1−8.
(78) Wu, X.; Xu, D.; Li, W.; Wang, T.; Cao, L.; Meng, J. Synthesis and luminescence of novel near-infrared emitting BaZrSi3O9:Cr3+ phosphors. *Luminescence* **2017**, *32*, 1554−60.
(79) Zhang, Y.; Liang, Y.; Miao, S.; Chen, D.; Yan, S.; Liu, J. Broadband near-infrared BaMSi3O9:Cr3+(M = Zr, Sn, Hf) phosphors for light-emitting diode applications. *Inorg. Chem. Front* **2021**, *8*, 5186−94.
(80) Yan, M.; Seto, T.; Wang, Y. Strong energy transfer induced deep-red emission for LED plant growth phosphor (Y,Ba)3(Al,Si)5O12: Ce3+, Cr3+. *J. Lumin.* **2021**, *239*, No. 118352.
(81) Nie, W.; Yao, L.; Chen, G.; Wu, S. H.; Liao, Z.; Han, L.; et al. A novel Cr3+-doped Lu2CaMg2Si3O12garnet phosphor with broadband emission for near-infrared applications. *Dalton Transactions* **2021**, *50*, 8446−56.
(82) Zhou, Y.; Li, X.; Seto, T.; Wang, Y. A High Efficiency Trivalent Chromium-Doped Near-Infrared-Emitting Phosphor and Its NIR Spectroscopy Application. *ACS Sustain Chem. Eng.* **2021**, *9*, 3145−56.
(83) Yao, L.; Shao, Q.; Xu, X.; Dong, Y.; Liang, C.; He, J.; et al. Broadband emission of single-phase Ca 3 Sc 2 Si 3 O 12 :Cr 3+ /Ln 3+ (Ln = Nd, Yb, Ce) phosphors for novel solid-state light sources with visible to near-infrared light output. *Ceram. Int.* **2019**, *45*, 14249−55.
(84) Jia, Z.; Yuan, C.; Li, R.; Sun, P.; Dong, R.; Liu, Y.; et al. Electron-phonon coupling mechanisms of broadband near-infrared emissions from Cr3+in the Ca3Sc2Si3O12garnet. *Phys. Chem. Chem. Phys.* **2020**, *22*, 10343−50.
(85) Li, R.; Liu, Y.; Yuan, C.; Leniec, G.; Miao, L.; Sun, P.; et al. Thermally Stable CaLu2Mg2Si3O12:Cr3+ Phosphors for NIR LEDs. *Adv. Opt Mater.* **2021**, *9*, 1−7.
(86) Zhang, L.; Wang, D.; Hao, Z.; Zhang, X.; Pan, G.; Wu, H.; Zhang, J.; et al. Cr3+-Doped Broadband NIR Garnet Phosphor with Enhanced Luminescence and its Application in NIR Spectroscopy. *Adv. Opt Mater.* **2019**, *7*, 1900185.

https://doi.org/10.1021/acsomega.3c08806
ACS Omega 2024, 9, 16880−16892

(87) Huang, W.; Zhang, J.; Fan, J.; Chen, P.; Zhou, L.; Zhang, X. From Ancient Blue Pigment to Unconventional NIR Phosphor: A Thermal-Stable Near-Infrared I/II Broadband Emission from Ca1−xSrxCu-Si4O10 Solid Solution. *Inorg. Chem.* **2024**, *63*, 812−823.
(88) Zhou, J.; Teng, Y.; Liu, X.; Ye, S.; Xu, X.; Ma, Z.; et al. Intense infrared emission of Er^3+ in Ca_8Mg(SiO_4)_4Cl_2 phosphor from energy transfer of Eu^2+ by broadband down-conversion. *Opt Express* **2010**, *18*, 21663.
(89) Chen, G.; Nie, W.; Zuo, J.; Li, Y.; Han, L.; Ye, X. A new broadband near-infrared emitting Mg2Al4Si5O18:Cr3+ phosphor for night-vision imaging. *Dalton Transactions* **2022**, *51*, 12576−84.
(90) Zou, X.; Zhang, H.; Li, W.; Zheng, M.; Molokeev, M. S.; Xia, Z.; Zheng, Y.; Li, Q.; Liu, Y.; Zhang, X.; Lei, B. Ultra-Wide Vis-NIR Mg2Al4Si5O18: Eu2+, Cr3+ Phosphor Containing Unusual NIR Luminescence Induced by Cr3+ Occupying Tetrahedral Coordination for Hyperspectral Imaging. *Adv. Opt Mater.* **2022**, *10*, 2200882.
(91) Kang, T. W.; Choi, Y. B.; Kang, C. H.; Park, Y. J.; Kim, J. H.; Bae, B.; Kim, S. W.; et al. Development of NaY9Si6O26:Yb3+ phosphors with high thermal stability for NIR anti-counterfeiting: study of its crystal structure and luminescent properties. *RSC Adv.* **2023**, *13*, 7597−7602.
(92) Smedskjaer, M. M.; Qiu, J.; Wang, J.; Yue, Y. Near-infrared emission from Eu-Yb doped silicate glasses subjected to thermal reduction. *Appl. Phys. Lett.* **2011**, *98*, 2011−4.
(93) Li, K.; Van Deun, R. Ca3La2Te2O12 :Mn4+, Nd3+, Yb3+ : An efficient thermally-stable UV/visible-far red/NIR broadband spectral converter for c-Si solar cells and plant-growth LEDs. *Mater. Chem. Front* **2019**, *3*, 403−13.
(94) Smith, R. P.; Hwang, AA-C; Beetz, T.; Helgren, E. Introduction to semiconductor processing: Fabrication and characterization of p−n junction silicon solar cells. *Am. J. Phys.* **2018**, *86*, 740−6.
(95) Zhou, D.; Song, H. Phosphors for Solar Cells. In *Phosphor Handbook: Novel Phosphors, Synthesis, and Applications*, 3rd ed.; Liu, R.-S., Wang, X.-J., Eds.; CRC Press: 2022; pp 651−688..
(96) Chen, J. Y.; Huang, C. K.; Hung, W. B.; Sun, K. W.; Chen, T. M. Efficiency improvement of Si solar cells using metal-enhanced nanophosphor fluorescence. *Sol. Energy Mater. Sol. Cells* **2014**, *120*, 168−74.
(97) Ho, W. J.; Yang, G. C.; Shen, Y. T.; Deng, Y. J. Improving efficiency of silicon solar cells using europium-doped silicate-phosphor layer by spin-on film coating. *Appl. Surf. Sci.* **2016**, *365*, 120−4.
(98) Ho, W. J.; Shen, Y. T.; Deng, Y. J.; Yeh, C. W.; Sue, R. S. Performance enhancement of planar silicon solar cells through utilization of two luminescent down-shifting Eu-doped phosphor species. *Thin Solid Films* **2016**, *618*, 141−5.
(99) Ho, W. J.; Shen, Y. T.; Liu, J. J.; You, B. J.; Ho, C. H. Enhancing photovoltaic performance using broadband luminescent down-shifting by combining multiple species of Eu-doped silicate phosphors. *Nanomaterials* **2017**, *7*, 340.
(100) Ho, W. J.; Deng, Y. J.; Liu, J. J.; Feng, S. K.; Lin, J. C. Photovoltaic performance characterization of textured silicon solar cells using luminescent down-shifting eu-doped phosphor particles of various dimensions. *Materials* **2017**, *10*, 21.
(101) Ho, W. J.; Bai, W. B.; Liu, J. J.; Shiao, H. P. Efficiency enhancement of single-junction GaAs solar cells coated with europium-doped silicate-phosphor luminescent-down-shifting layer. *Thin Solid Films* **2018**, *660*, 651−656.
(102) Yang, X.; Chen, J.; Zheng, S.; Chen, C. A downshifting Eu3+ doped glass embedded with concave pyramid microstructure to improve the efficiency of silicon solar cell. *Journal of Rare Earths* **2020**, *38*, 1158−64.
(103) Zhao, F.; Liang, Y.; Lee, J. B.; Hwang, S. J. Applications of rare earth Tb3+-Yb3+ co-doped down-conversion materials for solar cells. *Materials Science and Engineering: B* **2019**, *248*, No. 114404.
(104) Li, Y.; Wang, S.; Wang, Y. Designing a novel Eu2+-doped hafnium-silicate phosphor for an energy-down-shift layer of CsPbI3 solar cells. *Mater. Chem. Front* **2022**, *6*, 724−36.
(105) Parauha, Y. R.; Dhoble, S. J. Enhancement of photo-luminescence and tunable properties for Ce3+, Eu2+ activated Na2CaSiO4 downconversion phosphor: A novel approach towards spectral conversion. *J. Lumin.* **2022**, *251*, No. 119173.
(106) Lee, S.; Kim, C. U.; Bae, S.; Liu, Y.; Noh, Y. I.; Zhou, Z. Improving Light Absorption in a Perovskite/Si Tandem Solar Cell via Light Scattering and UV-Down Shifting by a Mixture of SiO2 Nanoparticles and Phosphors. *Adv. Funct. Mater.* **2022**, *32*, 2204328.
(107) Ho, W. J.; Chen, J. C.; Liu, J. J.; Ho, C. H. Enhancing luminescent down-shifting of Eu-doped phosphors by incorporating plasmonic silver nanoparticles for silicon solar cells. *Appl. Surf. Sci.* **2020**, *532*, No. 147434.
(108) Ho, W. J.; Feng, S. K.; Liu, J. J.; Yang, Y. C.; Ho, C. H. Improving photovoltaic performance of silicon solar cells using a combination of plasmonic and luminescent downshifting effects. *Appl. Surf. Sci.* **2018**, *439*, 868−75.
(109) Han, H. V.; Lin, C. C.; Lin, W. Y.; Tsai, Y. L.; Shen, T. L.; Kuo, H. C.; Yu, P. Enhance current density and power conversion efficiency in solar cells by using luminescent downshifting phosphors. *2014 IEEE 40th Photovoltaic Specialist Conference (PVSC)*; IEEE: 2014; pp 0022−0024. .
(110) Yang, G.-C.; Ho, W.-J.; Yeh, C.-W.; Sue, R.-S.; Shen, Y.-T.; Hu, C.-H.; Deng, Y.-J. Efficiency improvement of crystalline-Si solar cell using the combination of Europium doped silicate phosphors down shifting and SiO2 antireflective coating. *2015 Conference on Lasers and Electro-Optics (CLEO), San Jose, CA, USA*; Optica Publishing Group: 2015; paper JTu5A.50..
(111) Yang, G. C.; Ho, W. J.; Yeh, C. W.; Shen, Y. T.; Sue, R. S.; Hu, C. H.; Deng, Y. J. Electrical and optical characterization of crystalline-si solar cell with down shifting eu-doped silicate phosphors film depending on the coverage of phosphors particles using spin-on film process. *2015 IEEE 42nd Photovoltaic Specialist Conference (PVSC)*; IEEE: 2015; pp 1−3..
(112) Que, M.; Que, W.; Yin, X.; Shao, J. Enhanced sunlight harvesting of dye-sensitized solar cells through the insertion of a (Sr, Ba, Eu)2SiO4-TiO2 composite layer. *Mater. Res. Bull.* **2016**, *83*, 19−23.
(113) Ho, W. J.; You, B. J.; Liu, J. J.; Bai, W. B.; Syu, H. J.; Lin, C. F. Photovoltaic performance enhancement of silicon solar cells based on combined ratios of three species of europium-doped phosphors. *Materials* **2018**, *11*, 845.
(114) Ho, W. J.; Liu, J. J.; Ke, B. X. Characterization of Luminescent Down-Shifting Spectral Conversion Effects on Silicon Solar Cells with Various Combinations of Eu-Doped Phosphors. *Materials* **2022**, *15*, 452.

https://doi.org/10.1021/acsomega.3c08806
ACS Omega 2024, 9, 16880−16892